

# Superradiance-mediated photon storage for broadband quantum memory

Anindya Rastogi,<sup>1</sup> Erhan Saglamyurek,<sup>1,2</sup> Taras Hrushevskyi,<sup>1</sup> and Lindsay J. LeBlanc<sup>1,\*</sup>

<sup>1</sup>*Department of Physics, University of Alberta, Edmonton AB T6G 2E1, Canada*

<sup>2</sup>*Department of Physics and Astronomy, University of Calgary, Calgary, Alberta T2N 1N4, Canada*

Superradiance is a collective, coherent emission of photons from an excited ensemble of emitters, without any mediation by a photonic resonator or dipole-rephasing mechanism. In the regime where an atomic ensemble's superradiant behaviour enables photonic emission on timescales faster than the atoms' natural lifetime, we experimentally demonstrate a fast quantum memory protocol for broadband photonic signals in a cloud of laser-cooled rubidium atoms. We analyze the conditions for optimal operation of a superradiance-mediated memory, and show that for a given optical depth, this protocol offers the highest-bandwidth storage among protocols in the same system. High-bandwidth superradiance quantum memories provide unique opportunities for fast processing of optical and microwave photonic signals, with applications in large-scale quantum communication and quantum computing technologies.

Photonic emission from a collection of identical excited atoms under superradiant conditions is very different from that of a single-atom in free-space [1]. Comprehensive theoretical and experimental studies of superradiance [2–4] have led to the observation of various quantum optics phenomena like quantum beats [5], collective Lamb shifts [6, 7], and novel cavity quantum electrodynamics (QED) [8]. Initial studies focused on dense ensembles with sizes smaller than the excitation wavelength, whereas recent ones have shown that superradiance is also observable in large and dilute systems [9, 10]. In this respect, large atomic ensembles, by virtue of their high degree of experimental control, are especially amenable to superradiant effects: when an ensemble with moderate optical density ( $d > 1$ ) is coherently excited by a temporally short (broadband) and weak probe pulse, a burst of radiation is emitted along the forward direction of the incident probe [11–15]. The characteristic decay time of this emission is inversely proportional to the medium's optical depth and, for  $d \gg 1$ , can be much shorter than the spontaneous-emission lifetime of a single atom [5, 9, 10, 16–20]. This optical-depth dependence of the decay time is the hallmark of superradiant emission, which is in contrast with the collective decay of atomic dipoles among inhomogeneously broadened emitters (commonly referred to as the free-induction-decay (FID)) [21, 22].

In this paper, we show that rapid superradiant emission from an atomic ensemble can be harnessed for fast operation of optical quantum memories [23–25]. Inspired by theoretical proposals studying this regime [21, 26, 27], here we demonstrate a broadband spin-wave memory based on superradiance in a cloud of laser-cooled <sup>87</sup>Rb atoms featuring a homogeneously-broadened optical transition. We find that optimal memory is realized by matching the signal duration to the superradiant decay time of the system. Compared with other memory protocols, the superradiance-mediated memory offers the most relaxed optical depth requirement for broadband signals in systems where the absorption linewidths are

much narrower than the signal bandwidth to be stored. The inherently fast storage capability of this memory paves the way for bandwidth compatibility with conventional single-photon sources and high-speed quantum networks [28, 29].

To understand the principle of superradiance (SR) memory, consider an  $N$ -atom ensemble as the storage medium whose energy levels form a  $\Lambda$ -configuration, where two ground-state spin levels  $|g\rangle$  and  $|s\rangle$  are optically coupled to an excited level  $|e\rangle$ . We assume that all atoms initially populate  $|g\rangle$ , and that both  $|e\rangle \leftrightarrow \{|g\rangle, |s\rangle\}$  transitions are homogeneously-broadened, with Lorentzian lineshapes of characteristic width  $\Gamma$  and optical decoherence rates  $\gamma = \Gamma/2$ . In this system, a weak probe field (the optical signal to be stored) is resonant with the  $|g\rangle \leftrightarrow |e\rangle$  transition, and a strong control field (to initiate probe storage or recall) with Rabi frequency  $\Omega_c(t)$  drives the  $|e\rangle \leftrightarrow |s\rangle$  transition. Such a weak-excitation regime with resonant interactions between the optical fields and the ensemble is well-described by the coupled, linear Maxwell-Bloch equations [27, 30–32]

$$\partial_z \hat{E}(z, t) = i \frac{g\sqrt{N}}{c} \hat{P}(z, t), \quad (1)$$

$$\partial_t \hat{P}(z, t) = -\gamma \hat{P}(z, t) + ig\sqrt{N} \hat{E}(z, t) + \frac{i}{2} \Omega_c(t) \hat{S}(z, t), \quad (2)$$

$$\partial_t \hat{S}(z, t) = \frac{i}{2} \Omega_c^*(t) \hat{P}(z, t), \quad (3)$$

where we consider the 1D-propagation of optical fields along the medium from  $z = \{0, L\}$ . The photonic coherence  $\hat{E}(z, t)$  describes the spatial and temporal variation of the probe field, while  $\hat{P}(z, t)$  is the macroscopic polarization coherence of the  $|g\rangle \leftrightarrow |e\rangle$  transition and  $\hat{S}(z, t)$  is the spin-wave atomic coherence of the  $|e\rangle \leftrightarrow |s\rangle$  transition. The atom-probe coupling strength, in terms of optical depth, is  $g\sqrt{N} = \sqrt{cd\gamma/2L}$ , and we assume negligible relaxation between the levels  $|g\rangle$  and  $|s\rangle$ . For the input probe, we consider an exponentially rising pulse with a temporal profile of the form

$I_P(t) = I_0 e^{(t-\tau)/T_P} u(\tau-t)$  (where  $\tau$  is the abrupt switch-off time and  $u(t)$  is the Heavyside step function) and characteristic duration  $T_P \ll 1/\gamma$ . The associated probe bandwidth is  $B = 0.54/T_P$  (sec. SII), such that the memory operates in the broadband regime of  $2\pi B \gg \Gamma$ .

We divide the SR memory protocol into three stages: absorption, writing, and retrieval, which follow the general principles of “fast” lambda-type storage and readout [27, 30], and can also be extended to the “ladder”-type atomic configurations [33, 34]. In the absorption stage, the short incident probe causes the build-up of a polarization excitation across the entire ensemble (sec. SIA), on a timescale much shorter than the decoherence of the excited state, which can therefore be neglected ( $e^{-\gamma T_P} \approx 1$ ). This atomic polarization is maximized at the conclusion of the input pulse, leading to a subsequent reemission referred to as superradiance. We note that regardless of the line broadening mechanism (homogeneous/inhomogeneous), this type of reemission occurs naturally whenever a broadband pulse is absorbed by a spectral feature, whose linewidth is narrower than the bandwidth of the incident pulse [21]. As such, this absorption regime is different than in photon-echo and FID processes, where the probe bandwidths must be smaller than or comparable to the spectral bandwidth of the inhomogeneously broadened emitters [35].

In the writing stage, storage is achieved by converting the built-up polarization into a collective spin excitation via a control field applied just before the superradiant emission. For this  $\hat{P} \rightarrow \hat{S}$  mapping to be efficient, (i) the control duration ( $T_C$ ) must be much shorter than the superradiant decay time ( $T_C \ll T_{SR}$ ) ensuring a minimum leakage, and (ii) the control pulse-area must be  $\pi$ , ensuring a maximum transfer [21, 27, 36] (see also sec. SIB). The initial photonic-coherence remains stored in the atomic medium up to a time limited by the spin-wave decoherence. The retrieval stage is implemented by re-applying the  $\pi$ -control pulse to map the coherence from  $\hat{S} \rightarrow \hat{P} \rightarrow \hat{E}$ , and the probe is recovered in the output photonic mode.

A sample numerical simulation of the SR protocol is shown in Fig. 1. In the absorption stage, the polarization  $|P(z, t)|^2$  and photonic  $|E(z, t)|^2$  coherences grow in phase with each other, over the entire duration of the input probe (Fig. 1c). The polarization is maximised at the end of the probe pulse and, without intervention, leads to superradiant emission (green curve, Fig. 1a). However, this emission can be suppressed by applying a fast  $\pi$ -control pulse (gray curve, Fig. 1a) that maps the polarization onto the spin-wave coherence (Fig. 1c). Retrieval, after a desired storage time, is implemented by applying another  $\pi$ -pulse, that converts the stored spin-wave back into the output photonic signal (Fig. 1b,d).

To experimentally demonstrate an SR memory, we use an ensemble of  $N \approx 2 \times 10^8$   $^{87}\text{Rb}$  atoms, cooled to about  $35 \mu\text{K}$  via standard magneto-optical-trapping

(MOT) and polarization-gradient optical molasses techniques (Fig. 2a). We form the  $\Lambda$ -configuration on the “D2” line, with levels  $|g\rangle \equiv |5S_{1/2}, F = 1\rangle$ ,  $|s\rangle \equiv |5S_{1/2}, F = 2\rangle$ , and  $|e\rangle \equiv |5P_{3/2}, F' = 2\rangle$ . The probe and control fields, nearly resonant with the  $|g\rangle \leftrightarrow |e\rangle$  and  $|s\rangle \leftrightarrow |e\rangle$  transitions, are derived from two independent but phase-locked CW lasers. The probe and control fields are temporally shaped via an electro-optic modulator (EOM) and an acousto-optic modulator (AOM), respectively. The output probe is detected along the forward direction using a single-photon-detector (SPD).

To begin, we characterize the superradiant behaviour of our cold Rb ensemble ( $d \approx 9$ ) by sending short ( $T_P = 20 \text{ ns} < 1/\gamma = 54 \text{ ns}$ ) and weak probe pulses (containing  $\sim 10^3$  photons), with an increasing-exponential profile and a sharp switch-off (Fig. 2b). We observe that the probe is almost completely absorbed up to the switch-off time, and subsequently reemitted as superradiance, with characteristic time  $T_{SR} = 8 \text{ ns}$ . Note that this superradiant decay time is shorter than both the input duration and the spontaneous emission lifetime by factors of 2.5 and 3.5, respectively. A linewidth measurement of the probe transition ( $\Gamma$ ) further confirms that the probe bandwidth  $2\pi B > \Gamma$ , favouring the conditions for superradiance (Fig. 2b, inset).

Next, we verify the superradiant nature of the reemission by measuring the decay time of the emitted light as a function of optical depth (Fig. 2c). We alter the optical depth between 9 and 1.5 by performing a variable time-of-flight spatial expansion of the atomic cloud before the measurements. For each optical depth, we extract the  $1/e$  decay time of the peak intensity ( $T_{SR}$ ) by fitting to an exponential function  $I_{\text{norm}} = \exp(-t/T_{SR})$ . Figure. 2c, inset, shows that the decay time is  $d$ -dependent with values ranging between  $T_{SR} = (8.0 \pm 0.1) \text{ ns}$  and  $T_{SR} = (18.8 \pm 0.8) \text{ ns}$ , confirming the superradiant character. The inset also shows the efficiency of superradiant emission: the higher the  $d$ , the higher is the energy contained within the emitted signal and the shorter is the emission timescale, both suggesting that high memory efficiency requires large optical depth (leading to an efficient polarization build-up), as well as fast writing operation.

We now demonstrate the full operation of the SR spin-wave memory for short optical pulses. Limited by the power available in our setup ( $\approx 10 \text{ mW}$ ), the shortest write-read control pulses with near  $\pi$  pulse-area are Gaussian-shaped with a full-width-half-maximum (FWHM) duration of  $T_C = 20 \text{ ns}$ . Using these control pulses, we store a 20 ns long probe and retrieve it after 200 ns in the forward direction, as shown in Figure 2d. Furthermore, by changing the time separation between the write and read stages, we demonstrate storage up to  $6.2 \mu\text{s}$ . This yields the  $1/e$  memory lifetime of  $(4.2 \pm 0.3) \mu\text{s}$  (Fig. 2f), limited by the decoherence

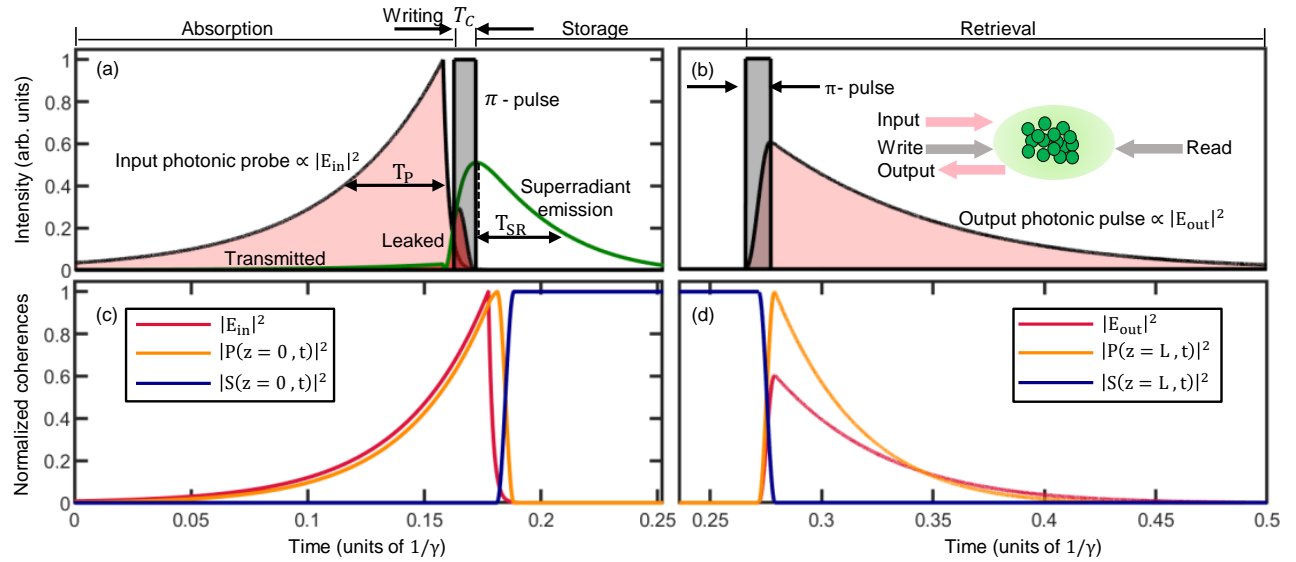


Figure 1. Superradiance (SR) memory protocol. (a,b) Timing sequence: a short input probe with duration  $T_P \ll 1/\gamma$  is absorbed by an ensemble with  $d \gg 1$ , and superradiantly reemitted with decay time  $T_{SR} \approx T_P$ . A  $\pi$ -control with a duration  $T_C \ll T_P$  significantly suppresses the superradiant emission, inducing photonic storage. Re-applying the  $\pi$ -pulse results in emission of the stored probe. (c) Time evolution of (normalized) photonic, polarization, and spin-wave coherences at  $z = 0$  leading to storage of the probe electric field ( $E_{in}(t) = E(z = 0, t)$ ). (d) Backward recall of the output photonic signal, simulated by inverting the spatial distribution of the stored spin-wave (i.e.  $S_b(L - z, t) = S(z, t)$ ). The simulation parameters  $[T_P, d, T_C, B, \Omega_C, \eta]$  are  $[0.037/\gamma, 50, 0.0074/\gamma, 45\Gamma/2\pi, 200\Gamma, 0.79]$ .

of the spin-wave due to the ambient magnetic fields. At 200 ns storage time, the overall memory efficiency ( $\eta^{exp}$ ) is 1.5%, which is significantly lower than the maximum achievable SR memory efficiency of 33%, calculated from eqns. (1-3) for  $d = 9$  and forward recall. Reaching this efficiency would require optimization of both probe and control fields.

An optimized probe corresponds to an exponentially rising temporal shape with a duration that matches the superradiant decay of the system, as elaborated upon later. We fulfill this shape condition reasonably well, however, our probe duration is longer than the measured superradiant decay time ( $T_{SR} = 8$  ns). By choosing the probe duration comparable to  $T_{SR}$ , the efficiency does increase to 3% (Fig. 2e), indicating that the main limitation comes from our non-optimized control fields. Although the area of our control pulses ( $0.85\pi$ ) is reasonably close to the optimal  $\pi$ -area, the control duration does not satisfy the condition  $T_C \ll T_{SR}$  for sufficiently fast writing. Therefore, a significant fraction of the built-up polarization is lost through superradiant emission before it is mapped onto the spin-wave. This loss of polarization coherence can be eliminated by using a nanosecond-long control pulse, which would then require two orders of magnitude higher intensity for the  $\pi$ -pulse area. In the absence of such intensity, it is still possible to alleviate the fast writing condition by extending the superradiance decay time at the expense of reducing the system's

optical-depth. Following such limited optimization, we achieve an efficiency of 5% by extending  $T_{SR}$  from 8 to 11 ns while reducing  $d$  from 9 to 6 (sec. SIII E).

With these proof-of-concept results at hand, we look forward and consider the optimality conditions for the SR protocol more broadly. Independent of any memory approach, the “optimality” criterion states that the maximum achievable memory efficiency ( $\eta_{opt}$ ) is universal and depends only on the medium’s optical depth [27, 30]. This criterion can be satisfied by implementing probe-and-control optimizations (specific to the protocol of interest) and the backward recall configuration (Fig. 1c,d), which together provide complete time reversal of the system dynamics.

Probe optimization in the SR protocol relies on both maximizing the polarization build-up and ensuring its proper spatial-distribution [ $P(z)$ ] in the absorption stage, which leads to an optimal spin-wave mode in the subsequent writing and readout stages. Such optimization is achieved by an input temporal profile that matches the time reversed replica of the superradiantly emitted pulse, both in shape and duration [22, 26, 37–39]. For a Lorentzian spectral feature (as in our cold Rb system, Fig. 2b, inset), the optimal shape of this probe is an exponentially-rising envelope with its duration given by the empirical relation [21, 36]

$$T_P^{opt} \approx \frac{1}{\Gamma} \left( \frac{1}{1 + \frac{d}{4}} \right), \quad (4)$$

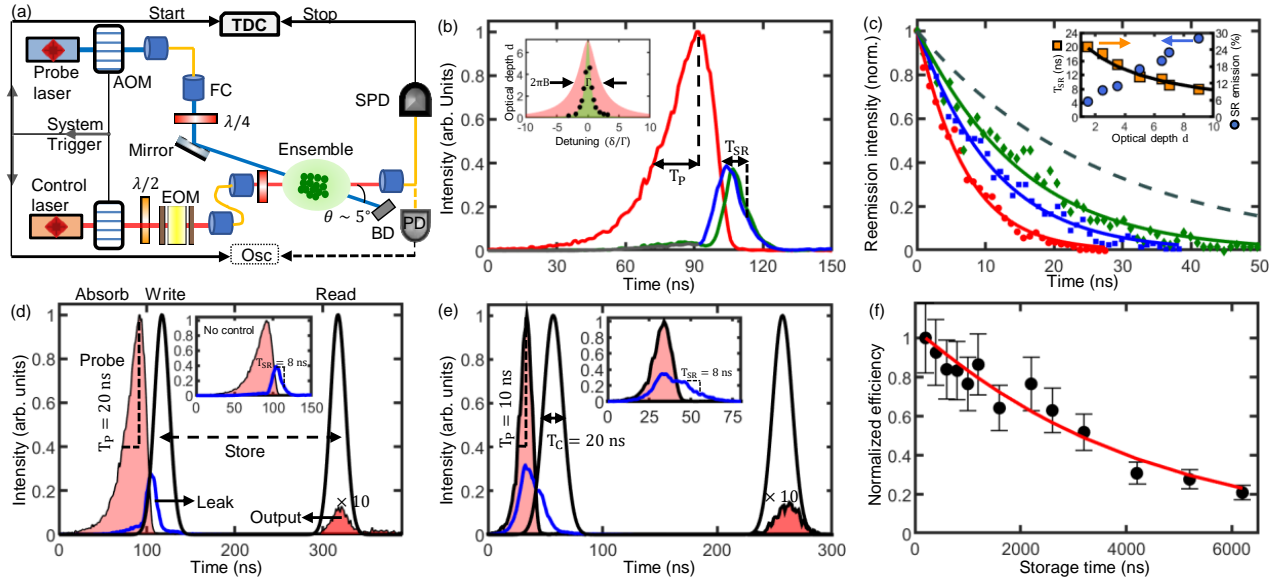


Figure 2. Demonstration of SR memory in cold  $^{87}\text{Rb}$  atoms. (a) Schematic of the setup with details in sec. SIII. (b) A weak probe (red) with  $T_P = 20$  ns is absorbed (gray : transmitted) and superradiantly reemitted (blue), with a  $1/e$  decay time  $T_{SR} = 8$  ns. Inset: probe's spectral profile (pink) with bandwidth  $B = 4\Gamma/2\pi$ , and linewidth  $\Gamma$  of the probe transition (green). (c) Decay of the superradiant emission intensity (normalized to its own maximum) for optical depths of 9 (red circles), 5 (blue squares), and 3.5 (green diamonds), with solid lines fit to the data. Black dashed line shows spontaneous emission decay (independent of  $d$ ). Inset: superradiant decay time  $T_{SR}$  and emission efficiency versus optical depth. Solid black line is fit of the measured  $T_{SR}$  values using eqn. (4), verifying that the probe duration for optimal SR memory matches the system's superradiant decay. (d,e) Storage and forward-retrieval of exponential probes with  $T_P = 20$  ns;  $B = 24$  MHz and the near-optimal  $T_P = 10$  ns;  $B = 39$  MHz, using Gaussian control fields with  $T_C = 20$  ns. Inset: SR emission without control. (f) Variation of memory efficiency with storage time, for a 10 ns probe. The fit gives a memory lifetime of  $4.2 \mu\text{s}$ .

which corresponds to the system's superradiant decay time, as verified numerically and experimentally (solid fit in Fig. 2c, inset). This optimized probe shape with  $T_P^{\text{opt}} \approx T_{SR}$  maximises the efficiency of superradiant emission, which in turn allows for optimal SR memory.

Control optimization in the SR protocol requires write-and-readout  $\pi$ -pulses with durations much shorter than the superradiant decay time, as discussed earlier. We numerically verify that for a square control pulse, a factor of ten times shorter duration i.e.  $T_C^{\text{opt}} \approx \frac{1}{10}T_{SR} \approx \frac{1}{10}T_P^{\text{opt}}$  is sufficient for reaching optimal efficiency at a given optical depth. Using equation (4), we can re-phrase this condition in terms of the required peak Rabi frequency ( $\Omega_C$ ) as  $\Omega_C \gg \gamma(1+d)$ , which is also stated by [27, 30] for fast writing and retrieval. For a Gaussian-shaped control as in our experiments, this condition translates into the required peak Rabi frequency of  $\Omega_C^{\text{opt}} = 24\gamma(1+d/4) = 75\gamma$  for  $d = 9$ , which is well above our experimental value of  $\Omega_C^{\text{exp}} = 4.8\gamma$ , resulting in an inefficient memory.

We now investigate the optical depth dependence of probe-duration (bandwidth), in terms of the adiabaticity parameter ( $T_P^{\text{opt}} d \gamma$ ) under the optimized probe-and-control conditions. Using equation (4) and for  $d \gg 1$ , this parameter is expressed as  $T_P^{\text{opt}} d \gamma \leq 2$ , which represents an operation regime opposite to that of adia-

batic memories, which are characterized by  $T_P^{\text{opt}} d \gamma \gg 1$  [27, 30, 32]. Therefore, SR memory falls into the class of non-adiabatic memories [35, 40], which are inherently suitable for optimal storage of broadband signals ( $2\pi B > \Gamma$ ). For example, in our Rb system ( $\gamma/2\pi = 3$  MHz) at  $d = 100$ , the adiabaticity parameter of SR memory renders optimal storage of pulses as short as  $T_P^{\text{opt}} = 1.1$  ns ( $B = 0.5$  GHz) with an efficiency of 90%. This would demand a square-shaped  $\pi$ -control with duration  $T_C = \frac{1}{10}T_{SR} = 0.11$  ns and Rabi frequency  $\Omega_C^{\text{opt}}/2\pi = 4.5$  GHz.

Finally, we make a performance comparison (efficiency, optical depth, bandwidth, and control-power) between SR and other memory approaches, including Autler-Townes-Splitting (ATS) [41–44] and electromagnetically-induced-transparency (EIT) [45–47], which are examples of non-adiabatic and adiabatic protocols, respectively. We base this comparison on the adiabaticity parameter, corresponding to  $T_P d \gamma = 2$  (SR);  $T_P d \gamma = 14$  (ATS); and  $T_P d \gamma = 60$  (EIT), for a broadband, exponential probe with  $T_P \ll 1/\gamma$ . For a given probe duration, the optical depth required for optimal SR efficiency is 7 times lower than in an ATS memory and 30 times lower than in an EIT memory (Fig. 3a). Equivalently, for a given optical depth, the bandwidth that can be optimally stored

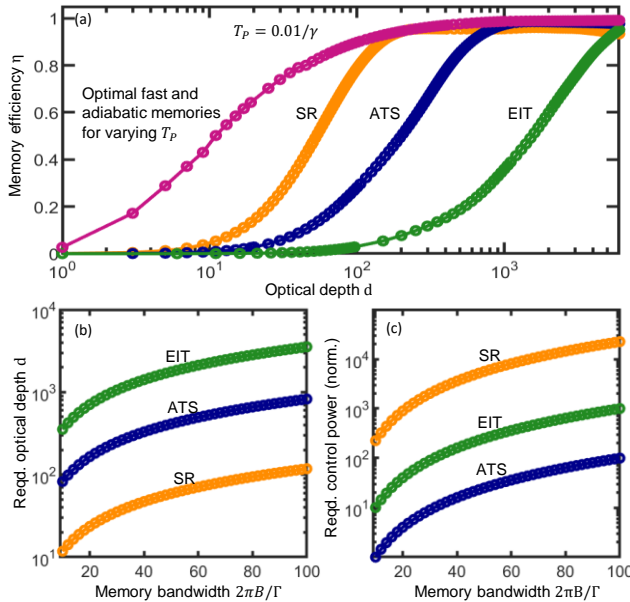


Figure 3. Theoretical analysis of SR memory versus ATS and EIT memories for storage of broadband light with optimized parameters  $[d, T_P, B, \Omega_C(t)]$  and backward recall. The ATS and EIT protocols are optimized using [41, 42]. (a) Numerically calculated memory efficiency versus optical depth for storage of an exponential probe with  $T_P = 0.01/\gamma$  ( $B = 166\Gamma/2\pi$ ), showing optimal operation at  $(d \approx 200, \eta \approx 0.93)$ ;  $(d \approx 1400, \eta \approx 0.96)$ ; and  $(d \approx 6000, \eta \approx 0.93)$  for the SR, ATS, and EIT protocols respectively. The universal optimal efficiency  $\eta_{\text{opt}}$  is obtained via optimal implementation of either protocol. (b,c) Optical depth and control power requirement versus memory bandwidth, so that near optimal operation is maintained ( $\eta \geq 0.9$ ). The control strength is normalized with respect to the ATS power required for  $B = 10\Gamma/2\pi$ .

using the SR protocol is higher than the corresponding bandwidth in the ATS and EIT protocols by the same factors, showing that SR protocol is the fastest among all protocols that are suitable for homogeneously-broadened transitions (Fig. 3b). Furthermore, Fig. 3c shows the scaling of the optimal peak control intensity ( $\propto \Omega_C^2$ ) as a function of probe bandwidth  $B$ : the optimal  $\Omega_C$  scales linearly as  $\Omega_{\text{ATS}} = 2\pi(0.6B)$ ;  $\Omega_{\text{EIT}} = 2\pi(2B)$ ; and  $\Omega_{\text{SR}} = 2\pi(9B)$ , implying that orders of magnitude larger control-power is required for the SR protocol. In sum, SR memory operates optimally at substantially lower optical depths than ATS and EIT memories, but its demand on control-power is significantly larger.

In conclusion, we experimentally demonstrated a broadband spin-wave memory based on the superradiance effect in a cold Rb gas. This memory approach offers the shortest pulse storage in systems with transition linewidths narrower than the signal bandwidth. In addition to conventional platforms like atomic gases and solid state systems, a high-performance SR memory could be implemented using Bose-Einstein condensates in

the originally conceived superradiant regime with large density and dimensions comparable to the excitation wavelength [1]. Beyond broadband quantum memories, our results may find use in the realizations of fast and efficient heralded single photon sources [36], atom-based optical processing [48], and superradiance-mediated dipole blockade effects [49, 50].

This work was supported by the University of Alberta; the Natural Sciences and Engineering Research Council, Canada (Grants No. RGPIN-04523-16, No. RGPIN-2014-06618, and No. CREATE-495446-17); the Alberta Quantum Major Innovation Fund; Alberta Innovates; and the Canada Research Chairs (CRC) Program. As researchers at the University of Alberta, we acknowledge that we are located on Treaty 6 territory, and that we respect the histories, languages, and cultures of First Nations, Métis, Inuit, and all First Peoples of Canada, whose presence continues to enrich our vibrant community.

\* Corresponding authors: lindsay.leblanc@ualberta.ca, rastogi1@ualberta.ca

- [1] R. H. Dicke, *Phys. Rev.* **93**, 99 (1954).
- [2] A. V. Andreev, V. I. Emel'yanov, and Y. A. Il'inskii, *Sov. Phys. - Uspekhi* **23**, 493 (1980).
- [3] M. Gross and S. Haroche, *Phys. Rep.* **93**, 301 (1982).
- [4] K. Cong, Q. Zhang, Y. Wang, G. T. Noe, A. Belyanin, and J. Kono, *J. Opt. Soc. Am. B* **33**, C80 (2016).
- [5] H. S. Han, A. Lee, K. Sinha, F. K. Fatemi, and S. L. Rolston, *Phys. Rev. Lett.* **127**, 073604 (2021).
- [6] M. O. Scully, *Phys. Rev. Lett.* **102**, 143601 (2009).
- [7] A. A. Svidzinsky and M. O. Scully, *Opt. Commun.* **282**, 2894 (2009).
- [8] M. O. Scully and A. A. Svidzinsky, *Science* **325**, 1510 (2009).
- [9] M. O. Araújo, I. Krešić, R. Kaiser, and W. Guerin, *Phys. Rev. Lett.* **117**, 73002 (2016).
- [10] S. J. Roof, K. J. Kemp, M. D. Havey, and I. M. Sokolov, *Phys. Rev. Lett.* **117**, 73003 (2016).
- [11] C. C. Kwong, T. Yang, M. S. Pramod, K. Pandey, D. Delande, R. Pierrat, and D. Wilkowski, *Phys. Rev. Lett.* **113**, 223601 (2014).
- [12] C. C. Kwong, T. Yang, D. Delande, R. Pierrat, and D. Wilkowski, *Phys. Rev. Lett.* **115**, 223601 (2015).
- [13] R. Pierrat, M. Chalony, D. Delande, and D. Wilkowski, *Front. Opt. 2012/Laser Sci. XXVIII* **84**, LTu11.3 (2012).
- [14] N. Dudovich, D. Oron, and Y. Silberberg, *Phys. Rev. Lett.* **88**, 4 (2002).
- [15] L. S. Costanzo, A. S. Coelho, D. Pellegrino, M. S. Mendes, L. Acioli, K. N. Casseiro, D. Felinto, A. Zavatta, and M. Bellini, *Phys. Rev. Lett.* **116**, 023602 (2016).
- [16] M. O. Scully, E. S. Fry, C. H. Ooi, and K. Wódkiewicz, *Phys. Rev. Lett.* **96**, 10501 (2006).
- [17] A. A. Svidzinsky, J. T. Chang, and M. O. Scully, *Phys. Rev. Lett.* **100**, 160504 (2008).
- [18] T. Bienaimé, M. Petruzzo, D. Bigerni, N. Piovella, and R. Kaiser, *J. Mod. Opt.* **58**, 1942 (2011).

[19] R. T. Sutherland and F. Robicheaux, *Phys. Rev. A* **93**, 23407 (2016).

[20] S. L. Bromley, B. Zhu, M. Bishof, X. Zhang, T. Bothwell, J. Schachenmayer, T. L. Nicholson, R. Kaiser, S. F. Yelin, M. D. Lukin, A. M. Rey, and J. Ye, *Nat. Commun.* **7**, 1 (2016).

[21] V. C. Vivoli, N. Sangouard, M. Afzelius, and N. Gisin, *New J. Phys.* **15**, 95012 (2013).

[22] A. Walther, A. Amari, S. Kröll, and A. Kalachev, *Phys. Rev. A* **80**, 012317 (2009).

[23] A. I. Lvovsky, B. C. Sanders, and W. Tittel, *Nat. Photonics* **3**, 706 (2009).

[24] K. Hammerer, J. Sherson, B. Julsgaard, J. I. Cirac, and E. S. Polzik, *Quantum Inf. with Contin. Var. Atoms Light* **82**, 513 (2007).

[25] K. Heshami, D. G. England, P. C. Humphreys, P. J. Bustard, V. M. Acosta, J. Nunn, and B. J. Sussman, *J. Mod. Opt.* **63**, 2005 (2016).

[26] A. Kalachev, *Phys. Rev. A* **76**, 043812 (2007).

[27] A. V. Gorshkov, A. André, M. D. Lukin, and A. S. Sørensen, *Phys. Rev. A* **76**, 033805 (2007).

[28] N. Sangouard, C. Simon, H. De Riedmatten, and N. Gisin, *Rev. Mod. Phys.* **83**, 33 (2011).

[29] H. J. Kimble, *Nature* **453**, 1023 (2008).

[30] A. V. Gorshkov, A. André, M. Fleischhauer, A. S. Sørensen, and M. D. Lukin, *Phys. Rev. Lett.* **98**, 123601 (2007).

[31] N. Sangouard, C. Simon, M. Afzelius, and N. Gisin, *Phys. Rev. A* **75**, 032327 (2007).

[32] J. Nunn, I. A. Walmsley, M. G. Raymer, K. Surmacz, F. C. Waldermann, Z. Wang, and D. Jaksch, *Phys. Rev. A* **75**, 011401 (2007).

[33] R. Finkelstein, E. Poem, O. Michel, O. Lahad, and O. Firstenberg, *Science Advances* **4**, eaap8598 (2018).

[34] K. T. Kaczmarek, P. M. Ledingham, B. Brecht, S. E. Thomas, G. S. Thekkadath, O. Lazo-Arjona, J. H. D. Munns, E. Poem, A. Feizpour, D. J. Saunders, J. Nunn, and I. A. Walmsley, *Phys. Rev. A* **97**, 042316 (2018).

[35] W. Tittel, M. Afzelius, T. Chanelière, R. L. Cone, S. Kröll, S. A. Moiseev, and M. Sellars, *Laser Photonics Rev.* **4**, 244 (2010).

[36] M. Ho, C. Teo, H. D. Riedmatten, and N. Sangouard, *New J. Phys.* **20**, 123018 (2018).

[37] A. Walther, A. Amari, S. Kröll, and A. Kalachev, *Phys. Rev. A* **80**, 012317 (2009).

[38] M. Stobińska, G. Alber, and G. Leuchs, *Europhys. Lett.* **86**, 14007 (2009).

[39] H. L. Dao, S. A. Aljunid, G. Maslennikov, and C. Kurtsiefer, *Rev. Sci. Instrum.* **83**, 83104 (2012).

[40] A. V. Gorshkov, A. André, M. D. Lukin, and A. S. Sørensen, *Phys. Rev. A* **76**, 033806 (2007).

[41] E. Saglamyurek, T. Hrushevskyi, A. Rastogi, K. Heshami, and L. J. LeBlanc, *Nat. Photonics* **12**, 774 (2018).

[42] A. Rastogi, E. Saglamyurek, T. Hrushevskyi, S. Hubele, and L. J. Leblanc, *Phys. Rev. A* **100**, 12314 (2019).

[43] E. Saglamyurek, T. Hrushevskyi, L. Cooke, A. Rastogi, and L. J. LeBlanc, *Phys. Rev. Res.* **1**, 22004 (2019).

[44] E. Saglamyurek, T. Hrushevskyi, A. Rastogi, L. W. Cooke, B. D. Smith, and L. J. LeBlanc, *New J. Phys.* **23**, 43028 (2021).

[45] M. Fleischhauer and M. D. Lukin, *Phys. Rev. Lett.* **84**, 5094 (2000).

[46] M. Fleischhauer and M. D. Lukin, *Phys. Rev. A* **65**, 022314 (2002).

[47] Y. F. Hsiao, P. J. Tsai, H. S. Chen, S. X. Lin, C. C. Hung, C. H. Lee, Y. H. Chen, Y. F. Chen, I. A. Yu, and Y. C. Chen, *Phys. Rev. Lett.* **120**, 183602 (2018).

[48] M. Mazelanik, M. Parniak, A. Leszczyński, M. Lipka, and W. Wasilewski, *npj Quantum Inf.* **5**, 22 (2019).

[49] A. Cidrim, T. S. do Espírito Santo, J. Schachenmayer, R. Kaiser, and R. Bachelard, *Phys. Rev. Lett.* **125**, 073601 (2020).

[50] L. A. Williamson, M. O. Borgh, and J. Ruostekoski, *Phys. Rev. Lett.* **125**, 073602 (2020).

# Supplemental Material for “Superradiance-mediated photonic storage for broadband quantum memory”

## SI. Evolution of coherences in superradiance protocol

The operation of superradiance protocol (Fig. 1a-d) is based on resonant interaction between an optically dense atomic ensemble and two electromagnetic fields, the “probe” and “control”. In the main text, we discuss its implementation in a  $\Lambda$ -type atomic system (see for example, Fig. 2a, inset) in terms of the exchange of coherences between the photonic ( $|E(z, t)|^2$ ) and the atomic ( $|P(z, t)|^2$ ,  $|S(z, t)|^2$ ) modes, using the Maxwell-Bloch equations (1) - (3). Following the mathematical framework of [21, 36], we obtain analytic expressions for  $P(z, t)$  and  $S(z, t)$  during the absorption, writing, and retrieval stages of the protocol. Further, since Maxwell-Bloch equations are applicable to both weak classical fields (inducing macroscopic atomic polarization) and single-photon fields (inducing a single excitation in the ensemble), in the following analyses, we drop the operator notation from the corresponding variables, treating them as fields and macroscopic observables.

### A. Absorption stage: Atomic-polarization generation from input probe

To understand how the atomic coherence is initially established, we examine the temporal and spatial profiles of the macroscopic polarization  $P(z, t)$  as it is generated in the medium during absorption of the input probe. In the absence of a control field ( $\Omega_C = 0$ ), equations (1)-(3) reduce to

$$\partial_z E(z, t) = \frac{ig\sqrt{N}}{c} P(z, t), \quad (S1)$$

$$\partial_t P(z, t) = -\gamma P(z, t) + ig\sqrt{N}E(z, t), \quad (S2)$$

with initial conditions given by the input photonic mode’s shape:  $E(z = 0, t) = \mathcal{E}_{\text{in}}(t) = E_P e^{t/T} u(-t)$ . Here,  $\mathcal{E}_{\text{in}}(t)$  is the electric field of the input probe, which has an amplitude  $\mathcal{E}_P$  and a  $1/e$  duration of  $T$  and  $u(-t)$  is the Heaviside unit step function. As discussed in the main text, this exponentially-rising temporal shape optimises both the amplitude as well as the spatial distribution of the built-up polarization, since it corresponds to the time-reversed impulse-response of the cold atomic ensemble (characterized by a Lorentzian lineshape), as in this study.

With the above definition of the input pulse and setting  $t = 0$  as the time at which the input is suddenly shut off, we consider the scenario in which absorption and the associated polarization build-up occurs for times

$t \leq 0^-$ , and for which subsequent re-emission or storage can occur at times  $t \geq 0^+$ . We assume that the probe field maintains its temporal shape during propagation through the medium ( $cT \gg L$ ) and that it is only changed by an attenuation of its amplitude. We also note that in the main text,  $T_P$  refers to the  $1/e$  duration of probe *intensity*, such that  $T_P = T/2$ .

Next, to study the temporal dynamics of the polarization, we convert eqns. (S1)-(S2) from the spatial to the complex spatial-frequency domain by taking the Laplace transform  $z \rightarrow u$  and denoting the transformed functions with “bars”:  $\bar{X}(u, t) = \mathcal{L}[X(u, t)] = \int dz e^{-uz} X(z, t)$ . In the transformed basis, the equivalents of (S1) and (S2) are

$$\bar{E}(u, t) = \frac{ig\sqrt{N}}{cu} \bar{P}(u, t) + \frac{1}{u} \mathcal{E}_{\text{in}}(t) \quad (S3)$$

$$\partial_t \bar{P}(u, t) = -\gamma \bar{P}(u, t) + ig\sqrt{N} \bar{E}(u, t). \quad (S4)$$

Inserting (S3) into (S4), we obtain a first-order linear differential equation in  $\bar{P}(u, t)$

$$\dot{\bar{P}}(u, t) + A \bar{P}(u, t) = \frac{ig\sqrt{N}}{u} \mathcal{E}_{\text{in}}(t), \quad (S5)$$

where

$$A \equiv \gamma + \frac{g^2 N}{cu} = \gamma \left( 1 + \frac{d}{2Lu} \right) \quad (S6)$$

and  $d = g^2 NL/2\gamma c$  is the on-resonant optical depth. Solving (S5) analytically, we find

$$\bar{P}(u, t) = \bar{P}(u, 0) e^{-At} + \frac{ig\sqrt{N}T}{u(1+AT)} \mathcal{E}_{\text{in}}(t).$$

Since polarization is induced only by the probe field, and no atoms are excited initially,  $\bar{P}(u, 0) = 0$  and

$$\bar{P}(u, t) = \frac{ig\sqrt{N}T}{u(1+AT)} \mathcal{E}_{\text{in}}(t). \quad (S7)$$

This expression describes generation of the polarization that is in phase with the input photonic field for a given spatial position  $z \rightarrow u$  (eg: see Fig. 1c for the polarization profile at  $z = 0$ ). While deriving (S7), we have assumed that the probe switch-off at time  $t = 0$  is instantaneous (i.e., the finite fall-time is neglected) such that the peak value of  $\bar{P}$  occurs at  $\bar{P}(u, t = 0)$ , when the probe amplitude is maximized.

Next, we consider the spatial variation of the polarization as the probe propagates through the atomic medium: we expect that the polarization, because it is in-phase with probe field, will undergo attenuation during

propagation. Using an approach very similar to the one above, we model the spatial variation of  $P$  along the propagation direction  $z$  at a given instant of time. Taking the Laplace transform in the time domain  $t \rightarrow \omega$  of equations (S1) and (S2), with tildes denoting the transformed variables, we find

$$\partial_z \tilde{E}(z, \omega) = \frac{ig\sqrt{N}}{c} \tilde{P}(z, \omega), \quad (\text{S8})$$

$$\tilde{P}(z, \omega) = \frac{1}{\omega + \gamma} \left[ ig\sqrt{N} \tilde{E}(z, \omega) + P(z, t = -\infty) \right]. \quad (\text{S9})$$

Since the medium does not contain any initial polarization,  $P(z, -\infty) = 0$  and equation (S9) can be substituted into (S8) to obtain:

$$\partial_z \tilde{E}(z, \omega) = -\frac{g^2 N}{c(\omega + \gamma)} \tilde{E}(z, \omega),$$

yielding

$$\tilde{E}(z, \omega) = e^{-g^2 N z / c(\omega + \gamma)} \tilde{E}(z = 0, \omega) \quad (\text{S10})$$

Equation (S10) represents the exponential decay in the probe-field amplitude along the propagation direction. Inserting it into (S9) gives the spatially decaying polarization profile

$$\tilde{P}(z, \omega) = \frac{ig\sqrt{N}}{\omega + \gamma} e^{-g^2 N z / c(\omega + \gamma)} \tilde{E}(z = 0, \omega) \quad (\text{S11})$$

Thus, at a fixed position  $z$  within the medium, the polarization amplitude grows in time, following the envelope of the probe field (S7), whereas at any fixed instant in time, the polarization amplitude exhibits an exponential decay along the medium length (S11).

### B. Writing stage: Polarization-to-spin-wave conversion

During absorption, the input-probe field imprints its phase pattern onto the atomic ensemble in the form of a polarization build-up over the entire probe duration. By applying a "write" control field immediately after the probe is absorbed (and when the photonic coherence has been completely converted to the polarization coherence), this atomic polarization is transferred into a long-lived spin-wave coherence of the atomic ensemble (Fig. 1a,c). In our formalism, absorption is maximized at  $t = 0$  with the value

$$\bar{P}(u, 0) = \frac{ig\sqrt{N}T}{u(1 + AT)} \mathcal{E}_p, \quad (\text{S12})$$

which serves as the source term upon which the write control acts. The transformation between the polarization

and spin coherences is governed by the Maxwell-Bloch equations (1)-(3), written again here for convenience:

$$\partial_z E(z, t) = \frac{ig\sqrt{N}}{c} P(z, t), \quad (\text{S13})$$

$$\partial_t P(z, t) = -\gamma P(z, t) + ig\sqrt{N} E(z, t) + \frac{i}{2} \Omega_c(t) S(z, t), \quad (\text{S14})$$

$$\partial_t S(z, t) = \frac{i}{2} \Omega_c(t) P(z, t), \quad (\text{S15})$$

where we have assumed  $\Omega_c$  to be real and ignored any spatial depletion of the control intensity (i.e.  $\Omega_c(z, t) = \Omega_c(0, t)$ ). We consider a square control pulse

$$\Omega_c(t) = \Omega_c, \quad 0 \leq t \leq T_c. \quad (\text{S16})$$

As the  $P \rightarrow S$  mapping occurs over a time-interval given by the control duration,  $T_c$  must be much shorter than the superradiant emission time  $T_{\text{SR}}$ , or else a significant portion of the built-up polarization is lost via superradiant emission. Taking the Laplace transform of (S13)-(S15) from  $z \rightarrow u$ :

$$\bar{E}(u, t) = \frac{ig\sqrt{N}}{cu} \bar{P}(u, t) + \frac{1}{u} E(z = 0, t) \quad (\text{S17})$$

$$\partial_t \bar{P}(u, t) = -\gamma \bar{P}(u, t) + ig\sqrt{N} \bar{E}(u, t) + \frac{i}{2} \Omega_c(t) S(u, t) \quad (\text{S18})$$

$$\partial_t \bar{S}(u, t) = \frac{i}{2} \Omega_c \bar{P}(u, t), \quad (\text{S19})$$

Since no photonic field  $E$  is present in the medium at the time when the write control is turned on ( $t = 0^+$ ),  $E(z = 0, t) = 0$ . Next, substituting (S17) and (S19) into the time-derivative of (S18), we obtain a second-order linear differential equation in  $\bar{P}(u, t)$

$$\ddot{\bar{P}}(u, t) + A \dot{\bar{P}}(u, t) + B \bar{P}(u, t) = 0, \quad (\text{S20})$$

where  $A \equiv \gamma + g^2 N / cu = \gamma(1 + d/2Lu)$  and  $B = \Omega_c^2/4$ . The roots of the characteristic equation in (S20), can be real or complex depending on the sign of the discriminant  $D = A^2 - 4B$  which is determined by the relative strengths of  $A$  and  $B$  coefficients. For the superradiance protocol the condition for fast storage and retrieval requires a strong driving control such that

$$\Omega_c \gg \gamma(1 + d),$$

implying  $\Omega_c \gg \gamma(1 + d/2Lu)$  and thus,  $4B \gg A^2$ . Roots of the characteristic equation are thus complex  $(-A/2 \pm i\Omega_c/2)$  giving a solution of the form

$$\bar{P}(u, t) = e^{-At/2} \left[ C(u) \cos \left( \frac{\Omega_c t}{2} \right) + D(u) \sin \left( \frac{\Omega_c t}{2} \right) \right]$$

for  $t \geq 0$ .

Applying the initial condition at  $t = 0$  (S12), the coefficient  $C(u) = P(u, t = 0)$ . Also, the fact that  $P(u, t = T_C)$  must ideally be 0 by the end of the control pulse suggests  $D(u) = 0$ . The expression for  $\bar{P}(u, t)$  during the writing stage is thus,

$$\bar{P}(u, 0 \leq t \leq T_C) = e^{-At/2} \cos\left(\frac{\Omega_c t}{2}\right) P(u, t = 0). \quad (\text{S21})$$

As can be seen, for  $\Omega_C T_C = \pi$  (i.e., a  $\pi$ -control-pulse with duration  $T_C$ ), no polarization remains in the medium by the end of control duration (i.e.,  $\bar{P}(u, T_C) = 0$ ) and is completely converted into the spin-wave  $\bar{S}(u, t = T_C) = \frac{i\Omega_c}{2} \int_0^{T_C} \bar{P}(u, t') dt'$ :

$$\bar{S}(u, T_C) = \frac{i\Omega_c}{A^2 + \Omega_c^2} \bar{P}(u, 0) [\Omega_c e^{-AT_C/2} + A] \quad (\text{S22})$$

Now, since we are in the regime of  $\Omega_C \gg A$ :  $\pi/T_C \gg A$  or  $AT_C/2 \ll 1$ , giving  $e^{-AT_C/2} \approx 1$ . Equation (S22) thus simplifies to:

$$\bar{S}(u, T_C) = iP(u, t = 0), \quad (\text{S23})$$

indicating that a lossless conversion of the polarization coherence into the spin-wave coherence can be achieved in the fast storage regime using a  $\pi$ -control-pulse.

### C. Converting the stored spin-wave back into polarization during retrieval

In previous subsection, we saw that a fast  $\pi$ -pulse can quickly act on the atomic polarization to convert it into the spin-wave with a unity-transfer-efficiency, thus effective storage of the input photonic coherence. The probe field remains stored as the spin-wave up to a time, referred to as the memory lifetime ( $T_{\text{Mem}}$ ), governed by the spin-wave decoherence processes. Re-applying the  $\pi$  pulse after a desired storage interval ( $T_S \leq T_{\text{Mem}}$ ), initiates the reversed mapping of  $S$  into  $P$  which then couples to the output photonic field (Fig. 1b,d). Assuming the absence of any decoherence mechanism that would otherwise degrade the spin-wave amplitude, we have the initial condition as  $\bar{S}(u, \tau) = \bar{S}(u, T_C)$  where  $\bar{S}(u, T_C)$  is the spin-wave generated by the end of the writing stage and  $\tau = T_C + T_S$  with all times measured relative to the the end of absorption process ( $t = 0$ ). The control field for readout is defined as

$$\Omega_c(t) = \Omega_c, \quad \tau \leq t \leq \tau + T_C, \quad (\text{S24})$$

so that the spin-to-polarization transfer occurs within the short duration of  $T_C$ . Taking the time derivative of (S19) and then inserting (S17) and (S18), we get a second order differential equation in  $\bar{S}(u, t)$

$$\ddot{\bar{S}}(u, t) + A\dot{\bar{S}}(u, t) + B\bar{S}(u, t) = 0, \quad (\text{S25})$$

where we used the fact that no photonic field is initially present at the time of readout; the  $A$  and  $B$  coefficients are defined as before. The condition for fast retrieval yields  $4B \gg A^2$ , giving a solution of the form

$$\bar{S}(u, \tau \leq t \leq \tau + T_C) = e^{-At/2} \cos\left(\frac{\Omega_c t}{2}\right) \bar{S}(u, t = T_C). \quad (\text{S26})$$

Again for a control pulse such that  $\Omega_C T_C = \pi$  during the interval  $t = T_C$ , the spin-wave in (S26) goes to 0 and is completely converted into the polarization coherence using  $\bar{P}(u, t) = (2/i\Omega_c) \partial_t \bar{S}(u, t)$ :

$$\bar{P}(u, t) = \frac{ie^{-At/2}}{\Omega_c} \left[ \Omega_c \sin\left(\frac{\Omega_c t}{2}\right) + A \cos\left(\frac{\Omega_c t}{2}\right) \right] \times \bar{S}(u, t = T_C),$$

which, for a  $\pi$ -pulse (and  $e^{-AT_C/2} \approx 1$ ) simplifies to

$$\bar{P}(u, \tau + T_C) = i\bar{S}(u, t = T_C), \quad (\text{S27})$$

indicating a lossless conversion of spin-wave into polarization at the time of readout.

## SII. Spectral bandwidth of input probe

We derive the Fourier-limited relationship between the rise time  $T_P$  and the bandwidth at full-width-half-maximum  $B$  of an excitation probe that has an exponentially rising temporal intensity of the form:

$$I(t) = e^{t/T_P} u(-t) + e^{-t/T_F} u(t), \quad (\text{S28})$$

where  $T_P$  and  $T_F$  are, respectively the  $1/e$  rise and fall times of the probe intensity, such that ideally  $T_F \ll T_P$ . The FWHM duration of such a pulse is given by  $T_{\text{FWHM}} = (T_P + T_F) \ln(2)$ . Taking the Fourier transform of eqn. (S28)

$$I(\omega) = \frac{1}{2\pi} \left[ \int_{-\infty}^0 e^{(\frac{1}{T_P} - i\omega)t} + \int_0^{+\infty} e^{-(\frac{1}{T_F} + i\omega)t} \right] dt = \frac{T_P + T_F}{2\pi} \left[ \frac{1}{1 - i\omega(T_P - T_F) + T_P T_F \omega^2} \right] \quad (\text{S29})$$

As an example, for numerical simulations in figures 1 and 3, we chose  $T_F = \frac{1}{10} T_P$ . Substituting in (S29),

$$I(\omega) = \frac{11}{2\pi} \frac{1}{T_P} \left[ \frac{1}{(\omega - i\frac{10}{T_P})(\omega + i\frac{1}{T_P})} \right],$$

which can be solved algebraically to obtain

$$|I(\omega)| = \frac{11T_P}{2\pi} \frac{1}{\sqrt{(100 + T_P^2 \omega^2)(1 + T_P^2 \omega^2)}},$$

which can then be numerically plotted to obtain the 3 dB frequency range as  $\omega_{3\text{ dB}} T_{\text{FWHM}} = 2.6$  or  $B = \omega_{3\text{ dB}}/2\pi = 0.54/T_P$  where  $T_{\text{FWHM}} = 0.76 T_P$ .

For the probe pulses in our experiment the fall time, limited by the electronic response of the arbitrary waveform generator which drives the probe-shaping EOM, was measured to be  $T_F^{\text{exp}} \approx 6$  ns. Hence, for a probe with  $T_P = 20$  ns and  $T_F^{\text{exp}} = \frac{1}{3}T_P$  (Fig. 2b,c,d), substituting in (S29), we get the magnitude response as

$$|I(\omega)| = \frac{2T_P}{\pi} \frac{1}{\sqrt{(9 + T_P^2 \omega^2)(1 + T_P^2 \omega^2)}},$$

giving  $\omega_{3\text{ dB}} T_{\text{FWHM}} = 2.75$  and thus,  $B = 0.47/T_P$  (using  $T_{\text{FWHM}} = 0.9T_P$ ). This corresponds to a bandwidth of 24 MHz, which is equivalent to  $4\Gamma/2\pi$  for our Rb atoms. Likewise, the 10 ns probe (Fig. 2e) corresponds to the bandwidth of  $B = 0.39/T_P = 39$  MHz =  $6.5\Gamma/2\pi$ .

### SIII. Experimental Setup and measurements

#### A. Cold Atom Preparation

An ensemble of laser-cooled  $^{87}\text{Rb}$  atoms serves as the medium for either probing the superradiant emission (fig. 2b,c) or for storing short optical pulses via the superradiant protocol (fig. 2d,e,f). The atoms are collected and cooled in a 3-dimensional retro-reflected magneto-optical-trap (MOT) operating on the D2 line. The MOT repump laser is frequency locked to the  $|F = 1\rangle \rightarrow |F' = 2\rangle$  transition using saturated absorption spectroscopy, at a detuning of -80 MHz. The repump beam is upshifted by +80 MHz using an acousto-optic-modulator (AOM) to make it resonant with the repump transition. The cooling (trapping) laser is frequency stabilized with respect to the repump laser using the offset beatnote locking technique such that it is detuned by  $\approx -180$  MHz from the  $|F = 2\rangle \rightarrow |F' = 3\rangle$  transition. The cooling beam is passed through a double-pass AOM stage which upshifts the frequency by +160 MHz, making it red-detuned from the cooling transition by  $\approx 3.5\Gamma$ . The 4 seconds of MOT cooling is followed by 5 ms of polarization-gradient optical molasses, at the end of which about  $2 \times 10^8$  Rb atoms are prepared in  $|F = 2\rangle$ . Time-of-flight (TOF) measurements of this cloud yield a size of 5 mm (Gaussian diameter at  $1/e^2$ ) and a temperature of 35  $\mu\text{K}$ .

A 3.5 ms optical-pumping stage follows molasses, wherein the repump beam is turned off but the cooling beam is kept on to off-resonantly transfer atoms from  $|F = 2\rangle$  into the  $|F = 1\rangle$  state, which serves as the initial population level ( $|g\rangle$ ) for the input probe field, providing an optical depth of  $d = 9$ . For datasets like the one in fig. 2c, a variable time-of-flight spatial expansion stage was introduced after the optical pumping stage, to controllably vary this optical depth.

#### B. Generation of probe and control fields

In our experiments, the probe and the control fields resonant with  $|F = 1\rangle \rightarrow |F' = 2\rangle$  and  $|F = 2\rangle \rightarrow |F' = 2\rangle$  transitions are derived from the MOT repump and cooling lasers respectively. To generate the probe pulse at the desired frequency, the CW beam from the repump laser is both gated and frequency-downshifted by 80 MHz using an AOM, such that the gated pulse is -160 MHz away from the probe transition. This gated pulse ( $\approx 200$  ns) is subsequently passed through a double-pass AOM which imparts a frequency shift of +160 MHz, thereby producing a resonant probe pulse. The resonant probe is then passed through an electro-optic intensity modulator (EOM) which shapes the gated pulse into an exponentially-rising temporal envelope with the desired rise time ( $T_P$ ). The CW cooling-laser-beam is passed through an AOM that generates Gaussian write and read temporal control pulses ( $T_C = 20$  ns), and imparts an additional frequency shift of -85 MHz making them resonant with the control transition. The RF oscillators driving the (gated) probe and control AOMs are amplitude controlled using a two-channel arbitrary waveform generator (AWG), while the probe-intensity EOM is driven directly from a separate AWG. The center frequency of probe pulse is set by adjusting the carrier frequency of the probe double-pass AOM, while the center frequency of control pulse is set by changing the beatnote offset between the repump and cooling lasers. AWGs are also used to adjust the relative timing positions between the probe and control fields.

After setting the amplitude (power), frequency, and timing of probe and control pulses, both beams are separately launched into the MOT chamber at an angular separation of  $\theta \approx 5^\circ$  inside the MOT cell. The probe is focused at the center of the atomic cloud with a  $1/e^2$  Gaussian diameter of 70  $\mu\text{m}$  while the control is collimated with 2.5 mm diameter. The initially linear polarization of each field is adjusted using  $\lambda/4$ -waveplates to maximise the atom-light interaction strength.

We perform experiments in the weak probe regime of  $N_P \ll N_A$ , where  $N_P$  is the total number of probe photons injected into the atomic cloud containing  $N_A$  atoms. For a single measurement run,  $N_P = n_P \bar{n}_{\text{in}}$  where  $n_P$  is the number of probe pulses injected with a mean photon number of  $\bar{n}_{\text{in}}$  in each pulse. Typical probe power before the MOT cell varied between 20 to 40  $\mu\text{W}$ . We place a series of neutral density filters (NDFs) along the path of the incident probe to attenuate its power by 30 dB, such that the  $\bar{n}_{\text{in}}$  reaching the MOT cell is  $\sim 10^3$  for operation in the linear optics regime. For the FWHM duration of 20 ns, the peak power of the Gaussian control pulse inside the MOT cell is 8 mW.

### C. Measurement and detection

The useful signals at the output of the probe arm include the input probe photons (in the absence of both atoms and control), superradiantly emitted probe photons (with atoms but without control), and stored-and-retrieved photons (with both atoms and control). We detect these signals using time-resolved photon counting measurements, enabled by a single-photon-detector (SPD) and a time-to-digital converter (TDC), in the form of histograms of the detected photon counts with respect to their arrival times. The SPD-TDC combination provided a better temporal resolution of the reemitted signal compared to the photodiode + oscilloscope pair in our setup.

In a single run, we perform measurements during a 1 ms detection window by sending a sequence of  $n_P = 1,000$  probe pulses (also write-read control if implementing SR memory) with a 1  $\mu\text{s}$ -separation between consecutive pulses, for each preparation of the atomic cloud. By repeating several such prepare-and-measure cycles ( $n_{\text{cyc}}$ ), signal integration over a large number of trials is achieved ( $n_{\text{cyc}}n_P$ ). Additional NDFs (providing up to 38 dB attenuation) are placed behind the MOT cell along the probe-output-path so that the average number of photons effectively reaching the SPD is below 1 ( $\approx 0.5\text{-}0.7$ ) thereby preventing the detector from going into the saturation mode (since  $\bar{n}_{\text{in}} \sim 10^3$ ). We calibrate  $\bar{n}_{\text{in}}$  by measuring probe counts in the absence of atomic cloud, following the procedure in our earlier studies [41, 43, 44].

Broadband memory demonstrations require strong control fields and so operation at the single-photon-level warrants heavy filtering of the scattered control light which would otherwise leak into the probe channel and produce spurious detection counts. In our current setup, the spatial mode of control field is separated from the probe by  $\theta = 5^\circ$ . This in combination with polarization-filtering and coupling of the probe-output into a single-mode-fiber yields  $\approx 80$  dB extinction of the scattered control, which is still not sufficient for a reliable single-photon-level operation with a high signal-to-noise ratio (SNR). Therefore, we implement the SR memory with  $\bar{n}_{\text{in}} \sim 1000$  such that the number of scattered photons per control pulse which leak into the probe channel (noise) is much smaller than the photons in the probe pulse (signal), giving an input SNR above 200. Accounting for the limited memory efficiency of the retrieved probe photons ( $\eta^{\text{exp}}$ ) due to our unoptimized control, we achieve an SNR of 10 at the output. We note that the control noise preventing single-photon-level operation is purely technical and not generated by the memory processes (unlike four-wave-mixing noise). In future implementations, this scattered leak can be eliminated by setting a larger separation angle between probe and control fields [43, 44].

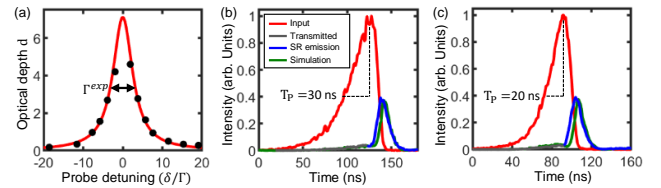


Figure S1. (a) Absorption linewidth of the probe transition ( $\Gamma^{\text{exp}}$ ). Black circles are the measured optical depth values with solid line as fit to the data (S30). (b,c) Estimation of peak optical depth by simulating the absorption-and-reemission measurements of short exponential probes using  $\Gamma^{\text{exp}}$ , yielding the peak optical depth of 9.

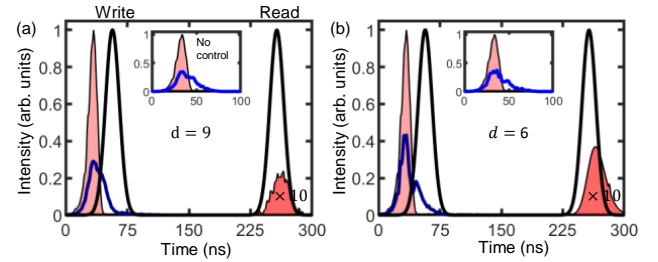


Figure S2. Storage followed by on-demand retrieval of a probe with  $T_P = 10$  ns using the SR protocol, at optical depths of (a)  $d = 9$  ( $T_{\text{SR}} = 8$  ns), and (b)  $d = 6$  ( $T_{\text{SR}} = 11$  ns). The overall memory efficiency values are 3 % and 5% respectively.

### D. Probe absorption linewidth and peak optical depth

To characterize the  $|5S_{1/2}, F = 1\rangle \leftrightarrow |5P_{3/2}, F' = 2\rangle$  probe transition we perform spectral measurements of the absorption linewidth ( $\Gamma^{\text{exp}}$ ) and the resonant optical depth ( $d_{\text{res}}$ ) for our Rb ensemble. Comparison of  $\Gamma^{\text{exp}}$  with respect to the natural linewidth would indicate whether there are additional broadening mechanism (eg: Doppler broadening) in our system. We send a sequence of 1000 square probe pulses, of duration 400 ns, at a fixed detuning ( $\delta$ ) and detect the probe transmission counts both without [ $I_{\text{in}}(\delta)$ ] and with [ $I_{\text{out}}(\delta)$ ] atoms. By performing such sequence over many cycles, reliable statistics can be obtained. The relatively long duration of the probe ( $T_P = 3.7/\gamma$ ) ensures no reemission occurs after absorption. These measurements are performed for values of  $\delta$  between -19 MHz to + 19 MHz with the optical depth in each case computed as  $d(\delta) = -\ln(I_{\text{out}}/I_{\text{in}})$ . By fitting a Lorentzian to the measured  $d$  values

$$d(\delta) = \frac{d_{\text{res}}}{1 + 4\left(\frac{\delta}{\Gamma}\right)^2}, \quad (\text{S30})$$

we extract the absorption linewidth  $\Gamma^{\text{exp}} = 2\pi \times (6.2 \pm 0.1$  MHz), and the peak optical depth  $d_{\text{res}} = 7 \pm 0.2$  (Fig. S1a). We note that the maximum measured OD

from our data is limited to  $\approx 5.6$  and hence less than what the fit in (S30) gives. We attribute this to the limited dynamic range of the SPD and thus exclude the data points near  $\delta = 0$  while performing the fit. The estimated value of  $\Gamma^{\text{exp}}$  agrees very well with the natural linewidth, confirming negligible effect of any inhomogeneous broadening and that the condition  $2\pi B > \Gamma^{\text{exp}}$  is well satisfied for observing superradiant emission, as in Fig. 2b.

Next, using the value of  $\Gamma^{\text{exp}}$ , we simulate our measurements for the absorption-and-reemission of short probe pulses, shown in Fig. S1b,c for  $T_P = 30$  ns ( $0.55/\gamma$ ) and 20 ns ( $0.37/\gamma$ ). A good agreement between experiments and simulations is obtained for a peak optical depth  $d_{\text{res}} = 9 \pm 1$  which is 25% higher than that obtained from spectral measurements. Since, the spectral measurements are carried out with pulses that are an order-of-magnitude larger, depletion of the atomic cloud during each pulse sequence can account for the observed discrepancy. Hence, the peak optical depth of our ensemble is closer to what we expect from the time-domain absorption measurements.

#### E. Optimizing the SR memory in our experiment

As discussed in the main text, our experimental SR memory efficiency is primarily limited by the non-optimal

writing stage: at  $d = 9$ , the superradiant emission drains the excited state within  $T_{\text{SR}} = 8$  ns whereas the control-induced polarization-to-spin-wave transfer occurs over an interval six times longer, given by the full duration of our experimental write control ( $2.25 \times T_C = 45$  ns). A comparison of probe's reemission profiles both in the absence and presence of the control field (Fig. 2d,e) suggests that a large fraction of the polarization coherence, accumulated during absorption, is lost via superradiant emission even when the control is present (referred to as "leakage"). Faster writing requires shorter control and in turn more power to maintain the  $\pi$ -area. Limited by the control power, another way to alleviate this leakage is to slow down the superradiant decay by lowering the system's optical depth. Figure S2 illustrates the storage-and-retrieval of a probe with near-optimal duration ( $T_P \approx T_{\text{SR}}$ ) at optical depths of 9 and 6, where at the lower  $d$ , reduction in the superradiance-induced leakage dominates over the increase in probe transmission, yielding a higher memory efficiency. We note however that this optimization is limited by the trade-off between the transmission and leakage losses: lowering the  $d$  further makes the probe-transmission dominant and reduces the efficiency.